Science of the Total Environment 613–614 (2018) 168–175

Contents lists available at ScienceDirect

Science of the Total Environment

journal homepage: www.elsevier.com/locate/scitotenv

OMI satellite observed formaldehyde column from 2006 to 2015 over Xishuangbanna, southwest China, and validation using ground based zenith-sky DOAS

Rui Liu [a,b], Tao Feng [c], Shanshan Wang [a,*], Chanzhen Shi [d], Yanlin Guo [a], Jialiang Nan [a], Yun Deng [e], Bin Zhou [a,f,**]

[a] Shanghai Key Laboratory of Atmospheric Particle Pollution and Prevention (LAP^3), Department of Environmental Science & Engineering, Fudan University, Shanghai 200433, China
[b] School of Resource and Environment, Yunnan University, Yunnan 650000, China
[c] School of Information Science, Yunnan University of Finance and Economics, Yunnan 650000, China
[d] Shanghai Institute of Measurement Testing Technology, Shanghai 200233, China
[e] Xishuangbanna Tropical Botanical Garden of Chinese Academy of Sciences, Yunnan 666100, China
[f] Fudan Tyndall Centre, Fudan University, Shanghai 200433, China

HIGHLIGHTS

- HCHO interannual variation from OMI during 2006–2015 is analyzed.
- Relationship between HCHO concentration and biomass burning, land use and land cover, and human activities is revealed.
- In situ observation with zenith-sky DOAS is developed to support the OMI results.

GRAPHICAL ABSTRACT

Zenith sky DOAS instrument was set in the XTBG to validate the OMI HCHO columns. OMI HCHO. Over the past ten years from 2006 to 2015, biogenic activity plays a role in controlling the background level of HCHO in Xishuangbanna, while biomass burning is the main driving force of high HCHO concentration. The area with high HCHO columns are covered with forest and shrub rather than the rubber trees which are typical vegetation in Xishuangbanna.

ARTICLE INFO

Article history:
Received 26 May 2017
Received in revised form 24 July 2017
Accepted 20 August 2017
Available online 14 September 2017

Editor: D. Barcelo

Keywords:
OMI HCHO
DOAS

ABSTRACT

Formaldehyde (HCHO) provides a proxy to reveal the isoprene and biogenic volatile organic compounds emission which plays important roles in atmospheric chemical process and climate change. The ground-based observation with zenith-sky DOAS is carried out in order to validate the HCHO columns from OMI. It has a good correlation of 0.71678 between the HCHO columns from two sources. Then we use the OMI HCHO columns from January 2006 to December 2015 to indicate the interannual variation and spatial distribution in Xishuangbanna. The HCHO concentration peaks appeared in March or April for each year significantly corresponding to the intensive fire counts at the same time, which illustrate that the high HCHO columns are strongly influenced by the biomass burning in spring. Temperature and precipitation are also the important influence factors in the seasonal variation when there is nearly no biomass burning. The spatial patterns over the past ten years strengthen the deduction from the temporal variation and show the relationship with land cover and

* Corresponding author.
** Correspondence to: B. Zhou, Shanghai Key Laboratory of Atmospheric Particle Pollution and Prevention (LAP^3), Department of Environmental Science & Engineering, Fudan University, Shanghai 200433, China.
E-mail addresses: shanshanwang@fudan.edu.cm (S. Wang), binzhou@fudan.edu.cn (B. Zhou).

http://dx.doi.org/10.1016/j.scitotenv.2017.08.210
0048-9697/© 2017 Published by Elsevier B.V.

Biomass burning
Land use and land cover
Population

land use, elevation and population density. It is concluded that the biogenic activity plays a role in controlling the background level of HCHO in Xishuangbanna, while biomass burning is the main driving force of high HCHO concentration. And forests are greater contributor to HCHO rather than rubber trees which cover over 20% of the land in the region. Moreover, uncertainties from HCHO slant column retrieval and AMFs calculation are discussed in detail.

© 2017 Published by Elsevier B.V.

1. Introduction

Formaldehyde (HCHO) is a kind of important trace component of urban atmosphere to exert significant impacts on photochemical activity by being a source photo-oxidants such as HO_2 and tropospheric ozone. Moreover, it has stimulating effects on human eyes, skin, respiratory mucosa and even cancers. HCHO is a high-yield product of various Non-methane volatile organic compounds (NMVOCs) which are emitted from anthropogenic, biogenic, and pyrogenic sources (Baek et al., 2014; Fu et al., 2007). Anthropogenic sources of VOCs are essential in urban environments while biogenic sources usually dominate for the areas with abundant vegetation, particularly in growing season (Palmer et al., 2003). On the other hand, HCHO from pyrogenic sources, is directly emitted from biomass burning and industrial processes, which can produce considerable HCHO (>5 ppbv) within the boundary layer, and further result in large HCHO enhancements in local. Besides, far away air transportation would be a non-ignorable HCHO source because of a long life time of VOC. In generally, it is well agreed that HCHO observation provides a proxy for BVOCs emission (Palmer et al., 2003) and pyrogenic NMVOCs, as well as better understanding of the factors affecting the emission variability.

We use the HCHO tropospheric columns retrieved from the Ozone Monitoring Instrument (OMI) between 2006 and 2015. Of the available sensors, OMI HCHO products have finer spatial and temporal resolution of 24 × 13 km^2 with global daily coverage than GOME-2, which has 80 × 40 km^2 resolution and global coverage one day and a half. And HCHO columns from OMI also have more satisfying slant column error than from SCIAMACHY and GOME-2 due to improved signal to noise. (Millet et al., 2008 and Curci et al., 2010) concluded that OMI HCHO could provide a quantitative top-down constraint on the European bottom-up VOC inventories from the Model of Emissions of Gases and Aerosol from Nature (MEGAN) and the chemistry-transport model CHIMERE. Boeke et al. (2011) combined aircraft measurements over the United States, Mexico, and the Pacific with a 3D model (GEOS-Chem) to evaluate formaldehyde column retrievals from OMI. It came to the conclusion of good correlation (R = 0.80) between OMI HCHO products and results from aircraft measurements and GEOS-Chem. Marais et al. (2012, 2014) found that the OMI HCHO columns follow closely the distribution of vegetation patterns in Africa and the isoprene emission from the central African rainforest is much lower than estimated by the MEGAN inventory. Barkley et al. (2013) used formaldehyde (HCHO) vertical column measurements from the SCIAMACHY and OMI to infer top-down isoprene emission estimates from tropical South America during 2006 and presented that median uncertainties were about 60–260% for SCIAMACHY, and 10–90% for OMI.

As an only existing tropical forests region with abundant ecosystem types in China, 87.9% area in Xishuangbanna is covered by vegetation (Liu et al., 2014), in form of forest (47.22%), rubber (26.12%), shrub (8.82%) and tea (4.04%). Particularly, in the study field, it has turned into a typical spot for land use and land cover changes as Xishuangbannan serves as the second biggest rubber plantation base in China in recent years (Liao et al., 2014). Geron et al. (2006) used enclosure measurements to quantify BVOC emission of 95 common plant species in and near the Xishuangbanna Tropical Biological Gardens. It is concluded that nearly half of the plant species studied emit isoprene at standardized rates exceeding 20 mg Cg^{-1} h^{-1} but *Hevea brasiliensis* is a light dependent monoterpene emitting species. However, specific researches on the atmospheric chemicals variation in this field are rarely conducted.

In this study we use the OMI HCHO columns from January 2006 to December 2015 to show the interannual variation trend and spatial distribution in Xishuangbanna. The possible influencing factors from the biogenic, anthropogenic and pyrogenic sources are discussed along with many auxiliary data. Furthermore, zenith-sky DOAS observation was carried out in order to validate the HCHO columns from space. The DOAS algorithm was applied to retrieve HCHO slant columns which are then turned into vertical columns by the air mass factors (AMF) calculation with SCIATRAN. Furthermore, the uncertainties of HCHO column results from space and ground-based observation, as well as AMFs determination are discussed in detail.

2. Data and methods

2.1. Field site

This study is focusing on the Xishuangbanna area (21°09′–22°36′N, 99°58′–101°50′), which was located at the south of Yunnan province in southwestern China, and at an elevation range from 587 m to 2429 m above sea level (Li et al., 2008). It covers a land area of 19,150 km^2, which is divided into three counties, i.e. Jinghong, Menghai and Mengla. It has a typical tropical monsoon climate with alternating distinct wet and dry season. Average annual precipitation in Xishuangbanna is 113.86–243.15 cm, among which over 80% occurs during wet season from May to October (Fang and Sha, 2006). Average annual temperature of this region is 10.9–22.6 °C (Liao et al., 2014).

2.2. OMI HCHO data

OMI HCHO L2G products with lower than 30% cloud fraction during January 2006 to December 2015 are selected. It contains several auxiliary parameters in each grid such as temporal, spatial, solar and viewing geometry, terrain height, cloud height, cloud fraction, ground-pixel quality flags, and extensive quality assurance information [*NASA README*].

HCHO fitting is performed in the spectral window 328.5–356.5 nm, within the UV-2 channel of the OMI instrument. Nonlinear least-squares was used as a retrieval algorithm to get HCHO slant columns which were converted to vertical columns by using air mass factors (AMFs) which accounts for the satellite viewing geometry, HCHO vertical distribution, surface reflectance, and atmospheric scattering by air-molecules, aerosols, and clouds. Uncertainty exists in every step during the retrieval. Over tropical South America, the uncertainties of a single HCHO slant column observation typically range from about 20–300% for SCIAMACHY, and 10–200% for OMI, for slant columns exceeding the global background (~4 × 10^{15} molecules cm^{-2}) (Barkley et al., 2013). The retrieval of HCHO suffers from the largest error among trace gas measurements from satellites, which typically range from 40 to 105% (Palmer et al., 2006; Kurosu et al., 2007).

2.3. Ground based DOAS measurement

Ground based zenith-sky DOAS observation is applied for a validation of OMI HCHO columns in the area during February 19 to April 28 in 2015. The instrument was set up in the rainforest sample plot

(21°57′N, 101°12′E, 756 m a.s.l., see Fig. 1) belonged to Xishuangbanna Tropical Botanical Garden (XTBG) of Chinese academy of sciences. The wavelength range of the Ocean Optics spectrometer we used is from 290 to 477 nm with a representative optical resolution of 0.75 nm (full width at half maximum, FWHM).

After comprehensive consideration from the previous research (Heckel et al., 2005; Barkley et al., 2013; Pinardi et al., 2013), the spectral fitting configuration in QDOAS was adopted in Table 1 (Pinardi et al., 2013).

In this study, the Zenith-DOAS data are the averaged values for all measurements within 2 h around the satellite overpass time at 13:30LT. We use the criterion of HCHO RMS <0.002 and the ratios of SCDs error to SCDs <20% to filter the fitting results.

2.4. Air mass factors determination

In this study, radiative transfer model SCIATRAN (v3.5.0) developed by IUP Bremen University is used to calculate the AMFs which are defined as the ratio of slant to vertical column densities, AMF = SCD/VCD. AMF determination has great influence on the uncertainty in HCHO retrievals (De Smedt et al., 2008; Barkley et al., 2012) and it depends on many factors such as HCHO profile, the aerosol loading, cloud fraction, cloud-top pressure, surface reflectance (Barkley et al., 2013). Considering the potential high HCHO concentration in the area with abundant vegetation, the ground based passive DOAS observation was performed during 28th April to 13th May in 2015. HCHO concentrations at the ground level ranging from 20 ppb to 30 ppb are measured and assumed to be homogenous within the boundary layer of 1 km. The HCHO vertical distribution profile above 1 km was taken from the HCHO profile in SCIATRAN database. Fig. 2(a) shows HCHO AMFs with different concentration within the boundary layer. Various aerosol optical thickness (AOT) are simulated by the combination of different parameters in the LOWTRAN aerosol database from SCIATRAN. Furthermore, the diurnal variation of O_4 SCDs was used to indicate the light path of the scattered light during the day. We could infer the day without cloud or less impacted by aerosols according to the U shape of diurnal O_4 variation.

Finally, a suitable set of HCHO AMFs is obtained under the scenario of rural aerosol loads with representative AOT of 0.49 at 337 nm for spring and the HCHO concentration of 20 ppb within the boundary height of 1 km.

Table 1
Baseline DOAS analysis settings used for HCHO slant column retrieval.

Parameter	Specification
Fitting interval	336–359 nm
Wavelength calibration	Calibration based on reference solar atlas (Chance and Kurucz, 2010)
Cross section	
HCHO	Meller and Moortgat (2000), 298 K
O_3	Bogumil et al. (2003), 223 KI_0-corrected
NO_2	Vandaelet al. (1996), 294 KI_0-corrected
BrO	Fleischmann et al. (2004), 223 K
O_4	Thalman and Volkamer (2013), 293 K
Closure item	Polynomial of order 5

2.5. Ancillary data

Ancillary data sets used in this research are temperatures and precipitations obtained from National Meteorological Information Center, China Meteorological Administration (http://data.cma.cn/), MODIS active fire products from NASA's Earth Observing System (https://earthdata.nasa.gov/active-fire-data), elevation data from the advanced ASTER GDEM v1 edition released by Geospatial Data Cloud platform (http://www.gscloud.cn), Landsat-8 OLI data (https://landsat.usgs.gov), and population data with one square kilometer resolution from the LandScan Global Population Database, produced by the Oak Ridge National Laboratories.

3. Results and discussion

3.1. HCHO VCDs of OMI and zenith-sky DOAS observation

In the following comparisons, the OMI HCHO data are selected for satellite pixels with distances <20 km. As can be seen from Fig. 4(a), HCHO columns from zenith-sky DOAS observation and OMI have a good positive correlation (R = 0.71678) during the observation period and the significant highs and lows from two sources are basically consistent in Fig. 3(b).

However, it is important to note that the ground-based HCHO columns are generally higher than those from OMI. Besides the uncertainties in the retrieval discussed in Section 2, different spatial resolution of OMI pixel and zenith-sky DOAS instrument can be the

Fig. 1. Observation location and zenith-sky DOAS instrument in Xishuangbanna.

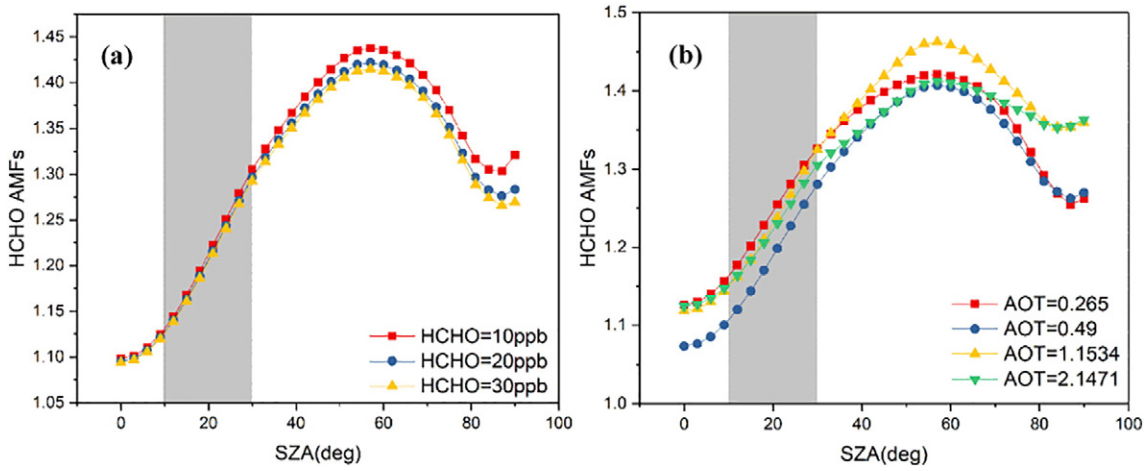

Fig. 2. HCHO AMFs with different concentration of 10, 20 and 30 ppb within the boundary layer in (a) and with different AOT scenarios in (b). The AMFs in (a) have very small gap in the SZA range of 10 to 30° in the grey band from 12:30 to 14:30 in Xishuangbanna. The AMFs in grey band vary within 10% under various AOT scenarios.

consistent interference. To clarify, zenith-sky DOAS instrument has smaller observation scope than MAX DOAS which results are always compared with the OMI products within a scope range from 30 km–50 km in previous study (Wang et al., 2017). However, there is nearly no reference of the corresponding scope for such a weak absorber trace gas HCHO between zenith-sky DOAS and OMI. Thus we use the scope of 20 km as a compromise solution in this study which means less valid pixels in the range to compare with. On the other hand, the zenith-sky DOAS instrument was set up in the rainforest while the OMI pixels around the observation spot covered with different types of features such as neighborhood, road and factory.

3.2. Temporal variation

Fig. 4 shows the interannual variation with monthly HCHO mean values during January 2006 to December 2015 from OMI in the range of Xishuangbanna. There is an outstanding HCHO concentration peak in March or April for each year, about 2 times higher than the other months' average. Previous studies indicated that biomass burning is the most significant source in spring over southern China (Chan et al., 2003; Duncan et al., 2003; Fu et al., 2007). Here, we use the active fire counts data from the Aqua and Terra MODIS instruments (Barkley et al., 2013; Baek et al., 2014) to map monthly biomass burning changes and distributions over the past ten years. Fig. 4 illustrates that the overwhelming fire counts in dry season from Februarys to Aprils are most likely responsible for causing the HCHO concentration peak for each year. However, the peak of fire counts in 2006 and 2007 is much larger than those in other years while the HCHO concentrations in the same two are not remarkable in ten years. It implies that other factors can be the contributor to the HCHO concentration peak at the same time. On the other hand, fire counts in Fig. 4 is not the only parameter to measure the biomass burning, fire radiative power (FRP) is also an important argument (Ichoku et al., 2008) which is discussed below.

In addition, many researches have figured out that biogenic VOC emissions are temperature dependent (Duncan et al., 2003; Bai and Baker, 2004; SITU Situ et al., 2010). In Fig. 4 the variation trends of HCHO concentrations and temperature are roughly aligned. However, the monthly averaged temperatures in different yeas vary in a small range of 2 °C–3 °C, which is hard to reveal the relationship with the HCHO concentration. Therefore, we perform the monthly variation analysis in 2010 of HCHO columns and temperatures and other potential factors.

Fig. 5 shows the monthly variation of OMI HCHO columns and potential influence factors in 2010. The biomass burning still dominate the HCHO concentration during February to the end of April. When the rainy season begins from May, HCHO columns continue to fall to

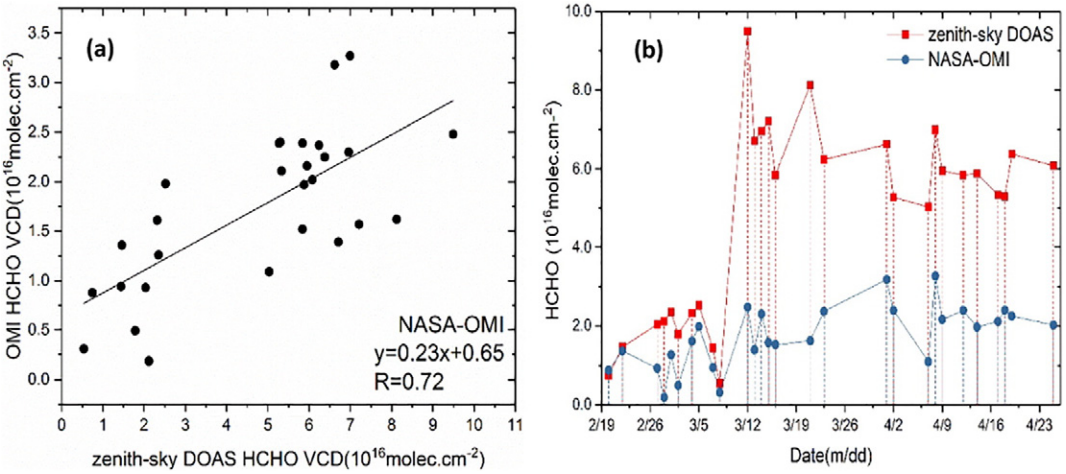

Fig. 3. Correlation in (a) and variation trend in (b) between HCHO VCDs from OMI and ground-based zenith-sky DOAS observation during 19th February to 28th April in 2015.

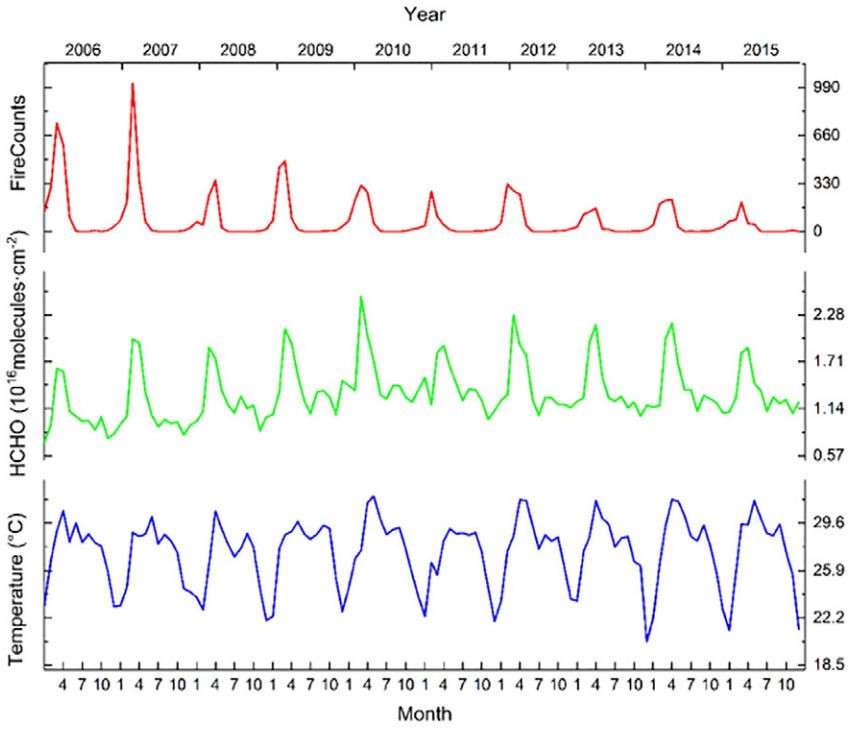

Fig. 4. Variation trend from January 2006 to December 2015 of monthly accumulated fire counts, monthly averaged OMI HCHO concentrations and monthly averaged temperature.

the lowest of the year while the precipitation reached to the highest in July, which indicates negative influence from precipitations in the area. The various trends of HCHO concentration and temperature are basically consistent from May to the end of October which make a response to the temperature dependent conclusion in previous studies. However, we cannot extrude the precipitation influence during the same period. It seems that the influence from temperature is covered up by the biomass and participation factors in this area, but still cannot be ignored.

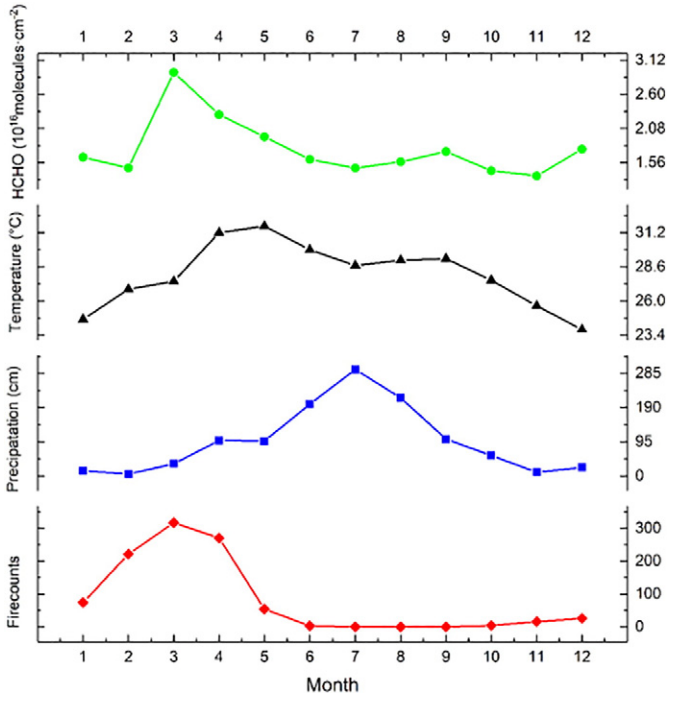

Fig. 5. Values of monthly averaged HCHO concentrations, temperatures and accumulated precipitation and fire counts in Xishuangbanna from January 2010 to December 2010.

3.3. Spatial distribution

Daily OMI HCHO columns in 2014 are processed with linear normalization method in GIS platform. The linear normalization transformation applies a linear function as follows to realize equal scaling in a dataset.

$$X_{norm} = (X - X_{min})/(X_{max} - X_{min})$$

Where x_{norm} is the normalized value from [0,1], x is the actual value, x_{max} and x_{min} are the max and min value in the dataset.

Here we use fire radiative power(FRP) in MW (megawatts) to characterize the biomass burning (Ichoku et al., 2008). The MODIS sensor is currently the only instrument that measures FRP globally on a daily basis. It is a twin sensor flying on two NASA Earth Observing System (EOS) satellites, with Terra crossing the equator at approximately 10:30 AM and 10:30 PM local time, and Aqua at approximately 1:30 AM and 1:30 PM local time. Thus we use the FRP data from Aqua at 1:30 PM allocated in Xishuangbanna from February to April in 2014 respectively in Fig. 6b, d, f.

The HCHO columns distributions in three months show a good coincidence with the FRP patterns which implies the main driving mechanisms in Xishuangbanna. It is mainly because of the biomass burning such as crop straw burning in spring season in these areas with more farmland (Li et al., 2008),especially in most part of Menghai county. However, there are some high HCHO concentration areas without any detected fire counts in mid-eastern Mengla and northern Jinghong in March, which reveal the other considerable HCHO sources at the same time.These areas are covered by abundant forests and shrubs which are discussed below. In addition, many fire counts from different days are detected in the northeast of Menghai in April (Fig. 6f) where HCHO concentration is at a lower level. The most possible reason is that the specific characteristics of the biomass fuel (e.g. ingredient,

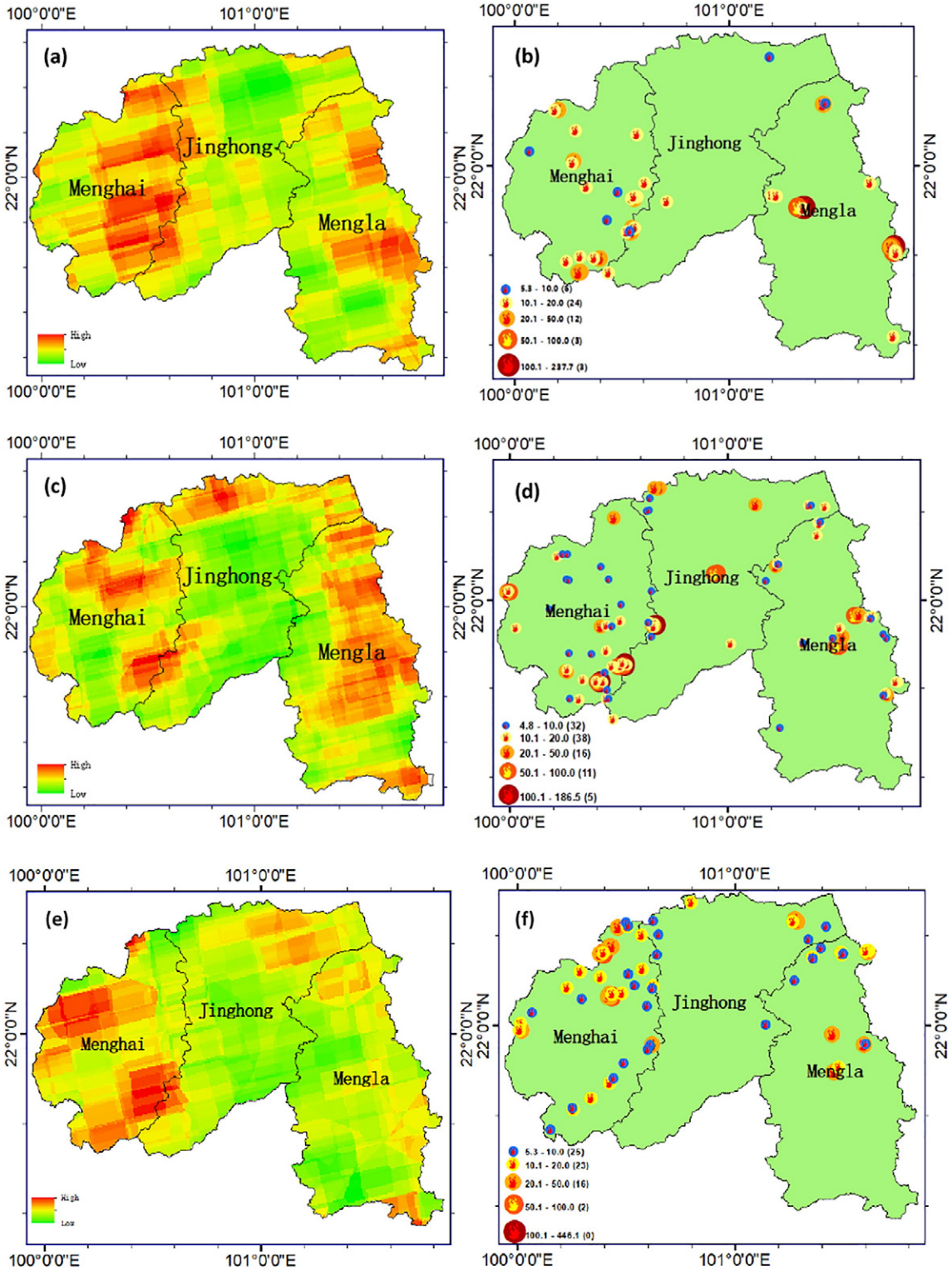

Fig. 6. Spatial pattern in Xishuangbanna in 2014 of normalized HCHO columns in (a) February, (c) March, (e) April, and corresponding fire radiative power in (b) February, (d) March, (f) April. The numbers in the bracket in (b), (d), (f) are the number of fire counts in the range of the FRP values respectively. They are found to range mostly between 5 and 20 MW because vegetation fires have essentially similar general combustion and energy release characteristics.

density, dryness) in the area is different from other place which bring the HCHO concentration raised.

From June, there is hardly any fire counts until the end of the year. It helps us to identify the biogenic source of HCHO without biomass burning influence. We get the land use and cover classification in Fig. 7b interpreted from Landsat-8 OLI data in 2014 as a proxy to show their influence to HCHO distribution in Fig. 7a preliminarily. The Kappa coefficient of the classification accuracy is 0.9214 which implies a reliable result, and it presents a good agreement with similar studies before in Xishuangbanna (Li et al., 2008; Li et al., 2011; Liao et al., 2014; Liu et al., 2014). Fig. 7b indicates that forests play a leading role of land cover types and rubber trees are the dominate land use type. Geron et

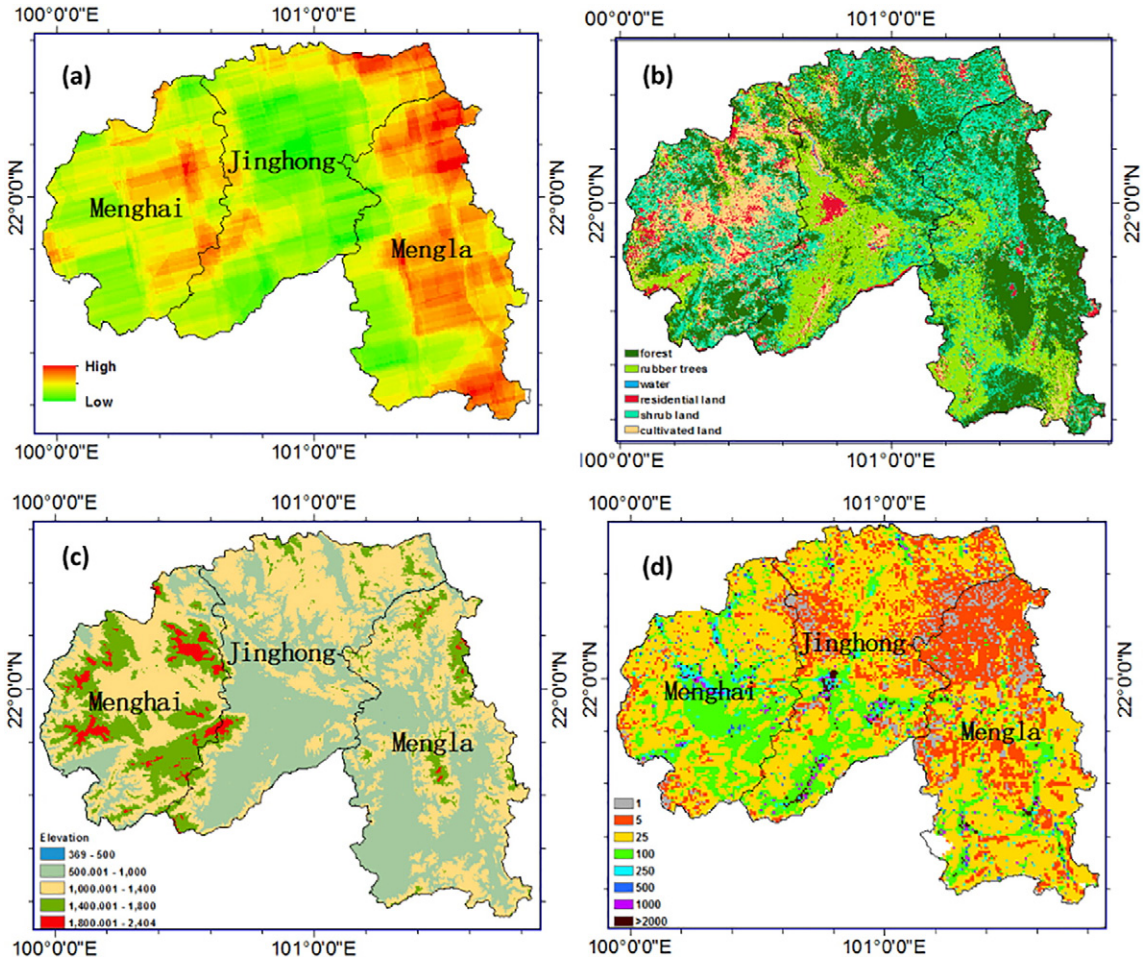

Fig. 7. Spatial pattern in Xishuangbanna of (a) normalized HCHO columns from June to December in 2014, (b) land use and land cover interpreted from Landsat-8 OLI data in 2014, (c) different altitude area, (d) population density with resolution of one square kilometers in 2014.

al. (2006) indicated that nearly half of the plant species studied emit isoprene at standardized rates exceeding 20 mg Cg^{-1} h^{-1} and verify that both the forest floor and canopy in Xishuangbanna can be sources of isoprene. Most units with high HCHO value are located in the area of forest, shrub and even cultivated land in Fig. 7b. Therefore, a further study is needed to match the specific species to the units with different HCHO concentration in order to highlight their contribution.

On the other hand, most rubber trees are planted in Jinghong and southern Mengla with lower HCHO concentrations in Fig. 7a. The conclusion from the Geron et al. (2006) that rubber trees in Xishuangbanna are monoterpene emitting species rather than isoprene, strengthen the result in this study.

Elevation distribution in Fig. 7c helps to verify the remote sensing interpretation result in Fig. 7b. They show that rubber trees are mainly distributed in the area with elevation below 1000 m (Li et al., 2008; Liu et al., 2014), where is in the southern Jinghong and southwestern Mengla. The dominated forest type such as montane broadleaved evergreen forest intensively grow above 900 m which cover the high HCHO value area at large in Fig. 6a (Zhu et al., 2015). And most ancient tea plants congregate in the region between the 1400 and 1800 m elevation (Liu et al., 2010), which corresponds to the sub-high HCHO extent in Fig. 6a.

Besides, it is important to note that the similar HCHO distribution can be seen in Figs. 7a and 6(a, c, e) which imply the biogenic resource has significant influence on the HCHO concentration even during the biomass burning seasons.

We also make the distribution of population density with high resolution of one square kilometers in Fig. 7d and to proxy the effect from the anthropogenic source causing by the industry and transportation (Baek et al., 2014). However, there is not an obvious correlation between the areas of high HCHO concentration and dense population. Especially in Jinghong city, the capital of Xishuangbanna with half of the population, it has lower HCHO columns than the other two counties.

From the analysis above, it can be inferred that the biogenic activity plays a role in controlling the background level of HCHO in Xishuangbanna, while biomass burning is the main driving force of high HCHO concentration, especially in spring season from February to April. And forests in the region are greater contributor to HCHO rather than rubber trees which cover over 20% of the land.

3.4. Conclusions and discussions

In order to reveal the HCHO interannual trend in Xishuangbanna from January 2006 to December 2015 and its possible influence factors, we use the HCHO columns from Aura OMI and other auxiliary data in order to perform their correlation analysis. As HCHO is the trace gas with low concentration in the atmosphere and errors/uncertainties from fitting specification and AMFs retrieval exist in OMI HCHO column, ground-based observation with zenith-sky DOAS technique was carried out during 19th February to 28th April in 2015 in order to validate the results from satellite. Criterion of retrieval results selection and AMFs determination are discussed in detail. Agreement with 0.7168

correlation index is acceptable because of the uncertainties in HCHO columns from both satellite and ground-based observation. Moreover, the ground-based results are generally higher than those from OMI. Over the past ten years from 2006 to 2015, the HCHO concentration peak appeared in March or April in each year shows a strong signal with the intensive biomass burning at the same time.

Spatial distribution of normalized HCHO columns in 2014 shows that most part of Menghai County and eastern Mengla County with higher HCHO concentrations are almost in the same area with vast fire counts from February to April. HCHO columns pattern from June to December with no fire counts indicates that there exist other factors to control background level of HCHO in Xishuangbanna. Comparing to the land use and land cover distribution interpreted from Landsat-8 OLI data in 2014, we find that forest and shrubs in the region are greater contributor to HCHO concentration rather than the rubber trees. The elevation data strengthen the result we conduct. Moreover, high resolution population distribution in the area is used to proxy the anthropogenic source in 2014. Overall, it comes to the conclusion that the biogenic activity plays a role in controlling the background level of HCHO in Xishuangbanna, while biomass burning is the main driving force of high HCHO concentration during February to April. The rubber trees do not make significant contribution to HCHO concentration, although they are the typical vegetation which cover over 20% of the land in Xishuangbanna.

Acknowledgements

This publication was supported by NSFC (41365010, 21477021, 41405117), the National Key Research Projects 2016 (2016YFC0200400) and the program for key laboratory in University of Yunnan Province.

References

Baek, K., et al., 2014. Validation of OMI HCHO data and its analysis over Asia. Science of the Total Environment 490:93–105. http://dx.doi.org/10.1016/j.scitotenv.2014.04.108.

Bai, J., Baker, B., 2004. Model simulation of isoprene emission flux in a tropical forest plantation of rubber trees. Acta Sci. Circumst. 24, 197–203.

Barkley, M.P., et al., 2012. Assessing Sources of Uncertainty in Formaldehyde Air Mass Factors Over Tropical South America: Implications for Top-down Isoprene Emission Estimates. 117:pp. 1–13. http://dx.doi.org/10.1029/2011JD016827.

Barkley, M.P., et al., 2013. Top-down isoprene emissions over tropical South America inferred from SCIAMACHY and OMI formaldehyde columns. J. Geophys. Res. Atmos. 118:6849–6868. http://dx.doi.org/10.1002/jgrd.50552.

Boeke, N.L., et al., 2011. Formaldehyde columns from the ozone monitoring instrument: urban versus background levels and evaluation using aircraft data and a global model. J. Geophys. Res. Atmos. 116 (5):1–11. http://dx.doi.org/10.1029/2010JD014870.

Chan, C.Y., et al., 2003. Characteristics of biomass burning emission sources, transport, and chemical speciation in enhanced springtime tropospheric ozone profile over Hong Kong. J. Geophys. Res. 108 (D1). http://dx.doi.org/10.1029/2001jd001555 ACH 3-1-ACH 3-13.

Chance, K., Kurucz, R.L., 2010. Journal of Quantitative Spectroscopy & Radiative Transfer An improved high-resolution solar reference spectrum for earth ' s atmosphere measurements in the ultraviolet , visible , and near infrared. J. Quant. Spectrosc. Radiat. Transf. 111 (9):1289–1295. http://dx.doi.org/10.1016/j.jqsrt.2010.01.036.

Curci, G., et al., 2010. Estimating European volatile organic compound emissions using satellite observations of formaldehyde from the ozone monitoring instrument. Atmos. Chem. Phys. 10 (23):11501–11517. http://dx.doi.org/10.5194/acp-10-11501-2010.

De Smedt, I., Müller, J.-F., et al., 2008. Twelve years of global observations of formaldehyde in the troposphere using GOME and SCIAMACHY sensors. Atmos. Chem. Phys. 8 (16): 4947–4963. http://dx.doi.org/10.5194/acp-8-4947-2008.

Duncan, B.N., et al., 2003. Interannual and seasonal variability of biomass burning emissions constrained by satellite observations. J. Geophys. Res. Atmos. 108 (D2). http://dx.doi.org/10.1029/2002JD002378 ACH 1-1-ACH 1-22.

Fang, Q., Sha, L., 2006. Soil respiration in a tropical seasonal rain forest and rubber plantation in Xishuangbanna, Y Unnan, Sw China. J. Plant Ecol. 30 (1), 97–103.

Fleischmann, O.C., Hartmann, M., Burrows, J.P., Orphal, J., 2004. New ultraviolet absorption cross-sections of BrO at atmospheric temperatures measured by time-windowing Fourier transform spectroscopy. J. Photochem. Photobiol. A Chem. 168: 117–132. http://dx.doi.org/10.1016/j.jphotochem.2004.03.026.

Fu, T.-M., et al., 2007. Space-based formaldehyde measurements as constraints on volatile organic compound emissions in east and south Asia and implications for ozone. J. Geophys. Res. 112 (D6):1–15. http://dx.doi.org/10.1029/2006JD007853.

Geron, C., et al., 2006. Volatile organic compounds from vegetation in southern Yunnan Province, China: emission rates and some potential regional implications. Atmos. Environ. 40 (10):1759–1773. http://dx.doi.org/10.1016/j.atmosenv.2005.11.022.

Heckel, A., et al., 2005. MAX-DOAS measurements of formaldehyde in the Po-Valley. Atmos. Chem. Phys. Discuss. 4 (1):1151–1180. http://dx.doi.org/10.5194/acpd-4-1151-2004.

Ichoku, C., et al., 2008. Global characterization of biomass-burning patterns using satellite measurements of fire radiative energy. Remote Sens. Environ. 112 (6):2950–2962. http://dx.doi.org/10.1016/j.rse.2008.02.009.

Kurosu, T.P., et al., 2007. Seasonally Resolved Global Distributions of Glyoxal and Formaldehyde Observed From the Ozone Monitoring Instrument on EOS Aura (January).

Li, Z., et al., 2008. Relation of land use and cover change to topography in Xishuangbanna, southweat China. J. Plant Ecol. 32 (5):1091–1103. http://dx.doi.org/10.3773/j.issn.1005-264x.2008.05.014.

Li, Y., Liu, G., Huang, C., 2011. Analysis of distribution characteristics of *Hevea brasiliensis* in the Xishuangbanna area based on HJ-1 satellite data. Sci. China (Information Science) 41, 166–176.

Liao, C., Li, P., Feng, Z., 2014. Area monitoring by remote sensing and spatiotemporal variation of rubber plantations in Xishuangbanna. Trans. Chin. Soc. Agric. Eng. 30 (22), 170–180.

Liu, B., et al., 2010. Geographic distribution, diversity and utilization of ancient tea plants from Xishuangbanna area in Yunnan. Chin. Agric. Sci. Bull. 26 (22), 344–349.

Liu, X., et al., 2014. Rubber plantations in Xishuangbanna: remote sensing identification and digital mapping. Resour. Sci. 36 (3), 233–244.

Marais, E.A., et al., 2012. Isoprene emissions in Africa inferred from OMI observations of formaldehyde columns. Atmos. Chem. Phys. 12 (14):6219–6235. http://dx.doi.org/10.5194/acp-12-6219-2012.

Marais, E.A., et al., 2014. Improved model of isoprene emissions in Africa using ozone monitoring instrument (OMI) satellite observations of formaldehyde: implications for oxidants and particulate matter. Atmos. Chem. Phys. 14 (15):7693–7703. http://dx.doi.org/10.5194/acp-14-7693-2014.

Meller, R., Moortgat, G.K., 2000. Temperature dependence of the absorption cross sections of formaldehyde between 223 and 323 K in the wavelength range 225-375 nm. J. Geophys. Res. 105 (D6), 7089–7101.

Millet, D.B., et al., 2008. Spatial distribution of isoprene emissions from North America derived from formaldehyde column measurements by the OMI satellite sensor. J. Geophys. Res. Atmos. 113 (2):1–18. http://dx.doi.org/10.1029/2007JD008950.

Palmer, P.I., et al., 2003. Mapping isoprene emissions over North America using formaldehyde column observations from space. J. Geophys. Res. 108 (D6). http://dx.doi.org/10.1029/2002JD002153 ACH 2-1-ACH 2-13.

Palmer, P.I., et al., 2006. Quantifying the Seasonal and Interannual Variability of North American Isoprene Emissions Using Satellite Observations of the Formaldehyde Column. 111:pp. 1–14. http://dx.doi.org/10.1029/2005JD006689.

Pinardi, G., et al., 2013. Erratum: MAX-DOAS formaldehyde slant column measurements during CINDI: intercomparison and analysis improvement. Atmos. Meas. Tech. 6 (2):167–185. http://dx.doi.org/10.5194/amt-6-219-2013.

Situ, S., et al., 2010. Impacts of errors in meteorological simulations on estimation of isoprene emission. Acta Sci. Circumst. 30 (12), 2382–2391.

Thalman, R., Volkamer, R., 2013. Temperature dependent absorption cross-sections of O2–O2 collision pairs between 340 and 630 nm and at atmospherically relevant pressure. Phys. Chem. Chem. Phys. 15:15371–15381. http://dx.doi.org/10.1039/c3cp50968k.

Vandaele, A.C., Hermans, C., Simon, P., Roozendael, M.V., 1996. Fourier Transform Measurement of NOa Absorption Cross-Section in the Visible Range at Room Temperature. J. Atmos. Chem. 25, 289–305.

Wang, Y., et al., 2017. Validation of OMI, GOME-2A and GOME-2B Tropospheric NO_2, SO_2 and HCHO Products Using MAX-DOAS Observations From 2011 to 2014 in Wuxi, China: Investigation of the Effects of Priori Profiles and Aerosols on the Satellite Products. Atmos. Chem. Phys. 17:5007–5033. http://dx.doi.org/10.5194/acp-17-5007-2017.

Zhu, H., et al., 2015. Studies on the forest vegetation of Xishuangbanna. Plant Sci. J. 33 (5), 641–726.